Mineralogical Magazine (2023), **87**, 10–17
doi:10.1180/mgm.2022.98

CAMBRIDGE UNIVERSITY PRESS

Article

Tombstoneite, a new mineral from Tombstone, Arizona, USA, with a pinwheel-like $Te^{6+}O_3(Te^{4+}O_3)_3$ cluster

Anthony R. Kampf[1]*, Stuart J. Mills[2], Robert M. Housley[3], Chi Ma[3] and Brent Thorne[4]

[1]Mineral Sciences Department, Natural History Museum of Los Angeles County, 900 Exposition Boulevard, Los Angeles, CA 90007, USA; [2]Geosciences, Museums Victoria, GPO Box 666, Melbourne 3001, Victoria, Australia; [3]Division of Geological and Planetary Sciences, California Institute of Technology, 1200 East California Boulevard, Pasadena, California 91125, USA; and [4]Earth Treasures, 3898 Newport Circle, Bountiful, UT 84010, USA

Abstract

The new mineral tombstoneite (IMA2021-053), $(Ca_{0.5}Pb_{0.5})Pb_3Cu^{2+}_6Te^{6+}_2O_6(Te^{4+}O_3)_6(Se^{4+}O_3)_2(SO_4)_2{\cdot}3H_2O$, occurs at the Grand Central mine in the Tombstone district, Cochise County, Arizona, USA, in cavities in quartz matrix in association with jarosite and rodalquilarite. Tombstoneite crystals are green pseudohexagonal tablets, up to 100 μm across and 20 μm thick. The mineral has a pale green streak and adamantine lustre. It is brittle with irregular fracture and a Mohs hardness of ~2½. It has one perfect cleavage on {001}. The calculated density is 5.680 g cm^{-3}. Optically, the mineral is uniaxial (–) and exhibits pleochroism: O = green, E = light yellow green; $O > E$. The Raman spectrum exhibits bands consistent with $Te^{6+}O_6$, $Te^{4+}O_3$, $Se^{4+}O_3$ and SO_4. Electron microprobe analysis provided the empirical formula $(Ca_{0.51}Pb_{0.49})_{\Sigma 1.00}Pb_{3.00}Cu^{2+}_{5.85}Te^{6+}_{2.00}O_6(Te^{4+}_{1.00}O_3)_6(Se^{4+}_{0.69}Te^{4+}_{0.24}S_{0.07}O_3)_2(S_{1.00}O_4)_2{\cdot}3H_2O$. Tombstoneite is trigonal, $P321$, $a = 9.1377(9)$, $c = 12.2797(9)$ Å, $V = 887.96(18)$ Å^3 and $Z = 1$. The structure of tombstoneite ($R_1 = 0.0432$ for 1205 $I > 2\sigma I$) contains thick heteropolyhedral layers comprising $Te^{6+}O_6$ octahedra, Jahn-Teller distorted $Cu^{2+}O_5$ pyramids, $Te^{4+}O_3$ pyramids and $Se^{4+}O_3$ pyramids. Pb^{2+} cations without stereoactive $6s^2$ lone-pair electrons are hosted in pockets in the heteropolyhedral layer. Pb^{2+} cations, possibly with stereoactive $6s^2$ lone-pair electrons, are located in the interlayer region along with SO_4 tetrahedra and H_2O groups. Within the heteropolyhedral layer, the $Te^{6+}O_6$ octahedra and the $Te^{4+}O_3$ pyramids form finite $Te^{6+}O_3(Te^{4+}O_3)_3$ clusters with a pinwheel-like configuration. This is the first known finite complex including both Te^{4+} and Te^{6+} polyhedra in any natural or synthetic tellurium oxysalt structure.

Keywords: tombstoneite, new mineral, tellurate, tellurite, selenite, sulfate, crystal structure, Raman spectroscopy, lone-pair electrons, Tombstone, Arizona, USA

(Received 7 May 2022; accepted 5 August 2022; Accepted Manuscript published online: 18 August 2022; Associate Editor: Irina O Galuskina)

Introduction

With the description of the current mineral and discounting 'girdite' and 'oboyerite', which are now discredited (Kampf *et al.*, 2017; Missen *et al.*, 2019), the Tombstone mining district has now yielded 12 new minerals (Table 1). All of these minerals, except cryptomelane, are tellurium oxysalts. Of the 11 tellurium oxysalts, four are tellurites with Te only in the 4+ oxidation state, six are tellurates with Te only in the 6+ oxidation state, and one is a mixed tellurite–tellurate, with Te in both the 4+ and 6+ oxidation states. The mixed tellurite–tellurate is the new mineral described herein and given the name tombstoneite.

Tombstoneite is named for the Tombstone mining district and the nearby town of Tombstone, Arizona, USA. The new mineral and name (symbol Tbs) were approved by the Commission on New Minerals, Nomenclature and Classification of the International Mineralogical Association (IMA2021–053, Kampf *et al.*, 2021). The description is based on one holotype specimen deposited in the collections of the Natural History Museum of Los Angeles County, Los Angeles, California, USA; catalogue number 76195.

Occurrence

Tombstoneite occurs at the Grand Central mine (31.70250, –110.06194) in the Tombstone district, Cochise County, Arizona, USA, ~1 km south of the town of Tombstone. The type specimen was originally collected by Sidney A. Williams and was obtained by one of the authors (BT) from Excalibur Minerals. The crystals were flagged as a probable new mineral first by Raman spectroscopy and then by SEM–EDS analysis at Caltech. The Grand Central mine exploits a Ag–Au–Pb–Cu–Zn deposit in which the ore, consisting principally of oxidised Ag- and Au-rich galena, occurs in faulted and fractured portions of a large dyke hosted by the Bisbee Group limestone. A good description of the history, geology and mineralogy of the Tombstone district has been provided by Williams (1980b). Tombstoneite occurs in cavities in quartz matrix in association with rodalquilarite and jarosite (Fig. 1).

*Author for correspondence: Anthony R. Kampf, Email: akampf@nhm.org
Cite this article: Kampf A.R., Mills S.J., Housley R.M., Ma C. and Thorne B. (2023) Tombstoneite, a new mineral from Tombstone, Arizona, USA, with a pinwheel-like $Te^{6+}O_3(Te^{4+}O_3)_3$ cluster. *Mineralogical Magazine* **87**, 10–17. https://doi.org/10.1180/mgm.2022.98

Table 1. Mineral species first described from the Tombstone mining district.

Mineral	Formula	Description	Structure
Adanite	$Pb_2(Te^{4+}O_3)(SO_4)$	Kampf *et al.* (2020)	Kampf *et al.* (2020)
Backite	$Pb_2AlTe^{6+}O_6Cl$	Tait *et al.* (2014)	Tait *et al.* (2014)
Cryptomelane	$K(Mn^{4+}_7Mn^{3+})O_{16}$	Richmond and Fleischer (1942)	Post *et al.* (1982)
Dugganite	$Pb_3Zn_3(AsO_4)_2(Te^{6+}O_6)$	Williams (1978)	Lam *et al.* (1998)
Emmonsite	$Fe^{3+}_2(Te^{4+}O_3)_3{\cdot}2H_2O$	Hillebrand (1885)	Pertlik (1972)
Fairbankite	$Pb^{2+}_{12}(Te^{4+}O_3)_{11}(SO_4)$	Williams (1979)	Missen *et al.* (2021)
Flaggite	$Pb_4Cu^{2+}_4Te^{6+}_2(SO_4)_2O_{11}(OH)_2(H_2O)$	Kampf *et al.* (2022)	Kampf *et al.* (2022)
Khinite	$Pb^{2+}Cu^{2+}_3[Te^{6+}O_6](OH)_2$	Williams (1978)	Cooper *et al.* (2008)
Murphyite	$Pb(Te^{6+}O_4)$	Yang *et al.* (2022)	–
Schieffelinite	$Pb_{10}Te^{6+}_6O_{20}(OH)_{14}(SO_4)(H_2O)_5$	Williams (1980a)	Kampf *et al.* (2012)
Tombstoneite	$(Ca_{0.5}Pb_{0.5})Pb_3Cu^{2+}_6Te^{6+}_2O_6(Te^{4+}O_3)_6(Se^{4+}O_3)_2(SO_4)_2{\cdot}3H_2O$	This study	This study
Winstanleyite	$TiTe^{4+}_3O_8$	Williams (1979)	Bindi and Cipriani (2004)

Physical and optical properties

Tombstoneite crystals are trigonal (pseudohexagonal) tablets, up to 100 μm across and up to 20 μm thick, that grow in subparallel stacks (Fig. 1). Tablets are flattened on {001}, exhibit the forms {100}, {001} and {101} (Fig. 2) and are twinned, probably by reflection on {001}. The mineral is green and transparent with adamantine lustre. The streak is pale green. No fluorescence was observed in either longwave or shortwave ultraviolet illumination. The Mohs hardness is ~2½ based upon scratch tests. Crystals are brittle with irregular fracture. There is one perfect cleavage on {001}. The calculated density based on the empirical formula and unit-cell parameters obtained from single-crystal X-ray diffraction data is 5.680 g cm^{-3} and that for the ideal formula is 5.668 g cm^{-3}. The density could not be measured because it exceeds that of available density liquids and there is an insufficient quantity for physical measurement. At room temperature, tombstoneite is soluble in dilute HCl.

Optically, tombstoneite is uniaxial (–). Due to the very small amount of material and the high indices of refraction, it was impractical to measure the indices of refraction. The Gladstone–Dale relationship (Mandarino, 2007) predicts an average index of refraction of 2.002 using the empirical formula. The mineral is pleochroic: O = green, E = light yellow green; $O > E$.

Fig. 1. Tombstoneite (green) on quartz with rodalquilarite (yellow green) and jarosite (beige to orange); field of view 0.56 mm across. Natural History Museum of Los Angeles County catalogue number 76195.

Raman spectroscopy

Raman spectroscopy was conducted on a Horiba XploRA PLUS using a 532 nm diode laser, 100 μm slit, 1800 gr/mm diffraction grating and a 100× (0.9 NA) objective. The spectrum from 4000 to 60 cm^{-1} recorded perpendicular to {001} are shown in Fig. 3. Note that the spectrum recorded parallel to {001} is essentially the same. The wavenumbers of the principal Raman bands are labelled in the figure.

The weak band at 1092 cm^{-1} is attributable to ν_3 SO_4 antisymmetric stretching and the moderately strong band at 971 cm^{-1} to ν_1 SO_4 symmetric stretching. The broad very weak band at ~870 cm^{-1} probably corresponds to the ν_1 symmetric stretching mode for SeO_3. The ν_3 SeO_3 antisymmetric stretching bands, typically occurring at ~800 to 750 cm^{-1} (see Mills *et al.*, 2014), are presumably hidden under the very strong band at 755 cm^{-1}, which can reasonably be assigned to ν_1 $Te^{4+}O_3$ symmetric stretching. The weaker band at 705 cm^{-1} may be due to ν_1 $Te^{6+}O_6$ symmetric stretching and the band at 680 cm^{-1} is most likely due to ν_3 $Te^{4+}O_3$ antisymmetric stretching (see Missen *et al.*, 2020). We do not feel confident in assigning modes to specific bands in the 600 to 300 cm^{-1} range; however, these all are likely to be due to various stretching and/or bending modes of $Cu^{2+}O_5$ and $Te^{6+}O_6$, as well as bending modes of SO_4, $Te^{4+}O_3$ and $Se^{4+}O_3$. Bands at lower wavenumbers are mostly due to lattice modes.

Chemical composition

Analyses (4 points) were performed at Caltech on a JEOL 8200 electron microprobe in wavelength dispersive spectroscopy mode. Analytical conditions were 15 kV accelerating voltage, 10 nA beam current and 5 μm beam diameter. Insufficient material is available for CHN analysis; however, the fully ordered structure unambiguously established the quantitative content of H_2O. The crystals did not take a good polish, which accounts for the low analytical total. Analytical data are given in Table 2.

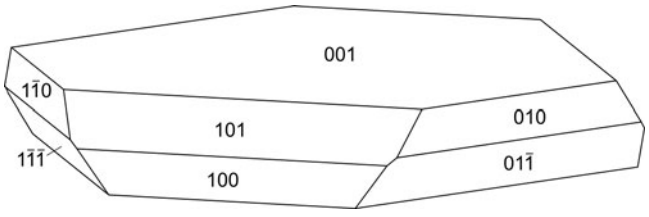

Fig. 2. Crystal drawing of tombstoneite, clinographic projection.

https://doi.org/10.1180/mgm.2022.98 Published online by Cambridge University Press

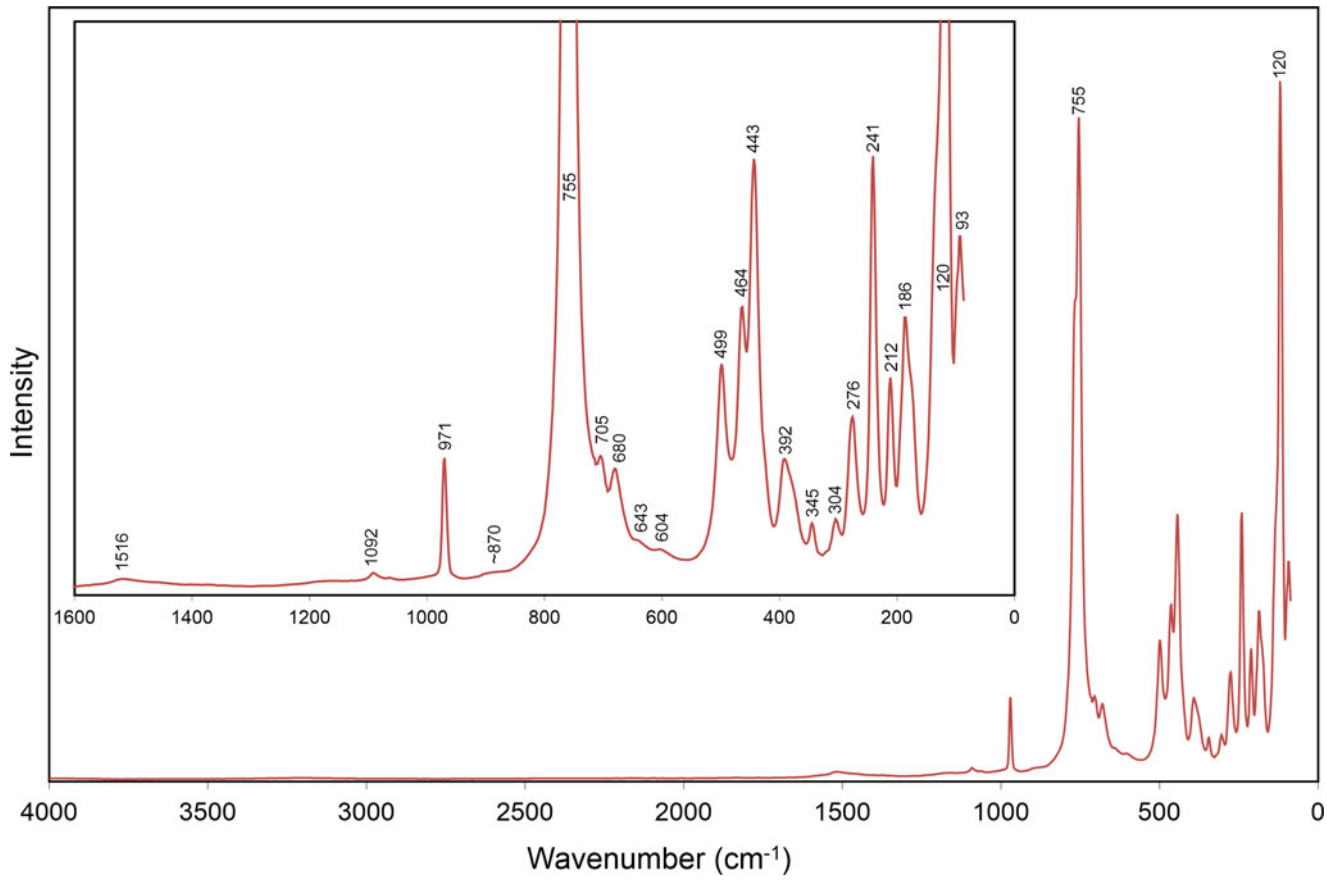

Fig. 3. The Raman spectrum of tombstoneite recorded with a 532 nm laser.

The empirical formula based on Te + Se + S = 12 and O = 41 apfu is $Ca_{0.51}Pb_{3.49}Cu^{2+}_{5.85}Te^{6+}_{2.00}Te^{4+}_{6.47}Se^{4+}_{1.39}S_{2.14}O_{41}H_{6.01}$ or assigned according to the structure $(Ca_{0.51}Pb_{0.49})_{\Sigma 1.00}Pb_{3.00}Cu^{2+}_{5.85}Te^{6+}_{2.00}O_6(Te^{4+}_{1.00}O_3)_6(Se^{4+}_{0.69}Te^{4+}_{0.24}S_{0.07}O_3)_2(S_{1.00}O_4)_2{\cdot}3H_2O$.

The simplified formula is $(Ca,Pb)Pb_3Cu^{2+}_6Te^{6+}_2O_6(Te^{4+}O_3)_6(Se^{4+}O_3)_2(SO_4)_2{\cdot}3H_2O$. Note that the Pb1 site in the structure appears to require the presence of approximately equal amounts of Pb and Ca for bond-valence balance at the site. For this reason, we provide an ideal formula with $Ca_{0.5}Pb_{0.5}$ at the Pb1 site. The ideal formula is $(Ca_{0.5}Pb_{0.5})Pb_3Cu^{2+}_6Te^{6+}_2O_6(Te^{4+}O_3)_6(Se^{4+}O_3)_2(SO_4)_2{\cdot}3H_2O$, which requires CaO 0.92, PbO 25.77, CuO 15.74, TeO_2 31.59, TeO_3 11.59, SeO_2 7.32, SO_3 5.28, H_2O 1.78, total 100 wt.%.

Table 2. Chemical composition (in wt.%) for tombstoneite.

Constituent	Mean	Range	S.D.	Standard
CaO	0.90	0.85–0.99	0.06	anorthite
PbO	24.33	23.37–25.35	0.82	PbS
CuO	14.51	14.37–14.63	0.12	Cu metal
TeO_2	(42.20)	41.98–42.63	0.30	Te metal
TeO_2*	32.24			
TeO_3*	10.96			
SeO_2	4.81	4.67–4.95	0.15	Se metal
SO_3	5.34	5.16–5.46	0.13	anhydrite
H_2O**	1.69			
Total	94.78			

* Allocated in accord with the structure.
** Based upon the crystal structure with Te+Se+S = 12 and O = 41 apfu.

X-ray crystallography and structure refinement

Powder X-ray diffraction was done using a Rigaku R-Axis Rapid II curved imaging plate microdiffractometer, with monochromatised Mo*K*α radiation. A Gandolfi-like motion on the φ and ω axes was used to randomise the sample and observed *d* values and intensities were derived by profile fitting using *JADE Pro* software (Materials Data, Inc.). The powder data are presented in Table 3.

Single-crystal X-ray studies were done on the same diffractometer and with the same radiation. The Rigaku *CrystalClear* software package was used for processing structure data, including the application of an empirical multi-scan absorption correction using *ABSCOR* (Higashi, 2001). The structure was solved using *SHELXT* (Sheldrick, 2015a). Refinement proceeded by full-matrix least-squares on F^2 using *SHELXL-2016* (Sheldrick, 2015b). All crystals are intergrowths of individuals stacked subparallel to {001}, some of which are apparently twinned by reflection on {001}. The crystal chosen for structure data collection consists of one principal individual and numerous smaller misaligned crystals. The data were of sufficient quality to allow the solution and refinement of the structure with anisotropic displacement parameters, although the presence of some reflection overlaps could not be avoided or properly accounted for, resulting in

https://doi.org/10.1180/mgm.2022.98 Published online by Cambridge University Press

Table 3. Powder X-ray diffraction data (d in Å) for tombstoneite.*

I_{obs}	d_{obs}	d_{calc}	I_{calc}	hkl
50	**12.36**	**12.2797**	**59**	**0 0 1**
18	7.94	7.9135	16	1 0 0
7	6.70	6.6519	4	1 0 1
5	6.11	6.1399	2	0 0 2
11	4.882	4.8510	10	0 1 2
19	4.578	4.5689	22	1 1 0
9	4.286	4.2821	10	1 1 1
8	4.109	4.0932	8	0 0 3
4	3.965	3.9567	5	2 0 0
15	3.775	3.7661	17	0 2 1
		3.6654	2	1 1 2
15	3.649	3.6357	14	1 0 3
17	3.335	3.3259	19	2 0 2
100	**3.056**	**3.0487**	**100**	**1 1 3**
		2.9910	7	2 1 0
42	**2.912**	**2.9061**	**56**	**2 1 1**
27	**2.867**	**2.8621, 2.8449**	**14, 16**	**1 0 4, 0 2 3**
34	**2.691**	**2.6889**	**37**	**1 2 2**
31	**2.639**	**2.6378**	**40**	**3 0 0**
		2.5790	4	0 3 1
11	2.560	2.5481	12	1 1 4
5	2.423	2.4255, 2.4150	3, 5	2 0 4, 2 1 3
		2.3456	2	0 1 5
		2.2459	2	2 2 1
		2.2173	2	0 3 3
		2.1606	3	1 3 1
21	**2.148**	**2.1423**	**19**	**2 1 4**
		2.1410	2	2 2 2
6	2.071	2.0667	6	3 1 2
8	2.052	2.0466	9	0 0 6
15	1.996	1.9948	13	2 2 3
7	1.952	1.9532	9	4 0 1
		1.9343	2	1 3 3
14	1.8975	1.8981	11	1 2 5
20	1.8738	1.8830, 1.8678	12, 13	0 4 2, 1 1 6
3	1.8185	1.8155	2	3 2 0
31	1.7918	1.7960, 1.7854	17, 17	3 2 1, 1 3 4
		1.7812	2	0 4 3
19	1.7399	1.7410	17	2 3 2
4	1.7154	1.7269	9	4 1 0
		1.7127	2	0 1 7
		1.6891	3	1 2 6
23	**1.6638**	**1.6630, 1.6596**	**16, 8**	**4 0 4, 3 2 3**
10	1.6369	1.6377, 1.6365	7, 5	1 1 7, 3 1 5
4	1.6114	1.6170	5	3 0 6
		1.6037	2	0 2 7
		1.5911	2	1 4 3
5	1.5659	1.5627	6	3 2 4
9	1.5401	1.5407	9	0 4 5
		1.5243	3	2 2 6
		1.5230	3	3 3 0
16	1.5157	1.5132	11	2 1 7
		1.5051	2	1 4 4
		1.4955	2	4 2 0
7	1.4834	1.4845, 1.4762	5, 5	2 4 1, 0 5 3
8	1.4612	1.4599	7	2 3 5
		1.4530	2	4 2 2
7	1.4276	1.4274	7	3 3 3
9	1.4120	1.4119	11	5 1 1
		1.3913	3	2 2 7
9	1.3854	1.3847	9	1 5 2
6	1.3667	1.3703, 1.3656	4, 4	3 1 7, 1 2 8

*Only calculated lines with $I > 1.5$ are listed. The eight strongest lines are given in bold.

most of the O atoms exhibiting significantly oblate ellipsoids. The Pb1 site was refined with joint occupancy by Pb and Ca and the Se site was refined with joint occupancy by Se and Te. All non-hydrogen sites were refined with anisotropic displacement parameters. Difference-Fourier synthesis did not suggest a possible location for the H atom. Data collection and refinement details are given in Table 4, atom coordinates and displacement parameters in Table 5, selected bond distances in Table 6 and bond-valence sums (BVS) in Table 7. The crystallographic information file has been deposited with the Principal Editor of *Mineralogical Magazine* and is available as Supplementary material (see below).

Table 4. Data collection and structure refinement details for tombstoneite.

Crystal data	
Structural formula	$(Ca_{0.50}Pb_{0.50})Pb_3Cu^{2+}_{5.90}Te^{6+}_2O_6(Te^{4+}O_3)_6(Se^{4+}_{0.84}Te^{4+}_{0.16}O_3)_2(SO_4)_2{\cdot}3H_2O$ [incl. unlocated H atom]
Crystal size (μm)	90 × 80 × 30
Space group	*P*321 (#150)
Unit cell dimensions (Å)	$a = 9.1377(9)$ Å
	$c = 12.2797(3)$
V (Å^3)	887.96(18)
Z	1
Density (for above formula) (g cm^{-3})	5.687
Absorption coefficient (mm^{-1})	28.73
Data collection	
Diffractometer	Rigaku R-Axis Rapid II
X-ray radiation / power	Mo$K\alpha$ ($\lambda = 0.71075$ Å)/50 kV, 40 mA
Temperature (K)	293(2)
F(000)	1324
θ range (°)	3.06 to 27.48
Index ranges	$-11 \le h \le 9$, $-11 \le k \le 10$, $-15 \le l \le 15$
Refls collected / unique	5529 / 1328; $R_{int} = 0.0968$
Reflections with $I > 2\sigma I$	1205
Completeness to θ = 27.48°	99.5%
Refinement details	
Refinement method	Full-matrix least-squares on F^2
Parameters / restraints	101 / 0
GoF	1.101
Final R indices [$I_o > 2\sigma I$]	$R_1 = 0.0432$, $wR_2 = 0.0846$
R indices (all data)	$R_1 = 0.0499$, $wR_2 = 0.0910$
Abs. structure parameter	0.023(12)
Extinction coefficient	0.0005(2)
Largest diff. peak / hole (e/A^3)	+2.97 / −2.80

*$R_{int} = \Sigma|F_o^2 - F_o^2(\text{mean})|/\Sigma[F_o^2]$. GoF = $S = \{\Sigma[w(F_o^2 - F_c^2)^2]/(n-p)\}^{1/2}$. $R_1 = \Sigma||F_o| - |F_c||/\Sigma|F_o|$. $wR_2 = \{\Sigma[w(F_o^2 - F_c^2)^2]/\Sigma[w(F_o^2)^2]\}^{1/2}$; $w = 1/[\sigma^2(F_o^2) + (aP)^2 + bP]$ where a is 0, b is 24 and P is $[2F_c^2 + \text{Max}(F_o^2, 0)]/3$.

Description and discussion of the structure

The asymmetric unit of the structure of tombstoneite (Fig. 4) includes one SO_4 sulfate tetrahedron, one Jahn-Teller distorted $Cu^{2+}O_5$ tetragonal pyramid [with four equatorial O atoms (O_{eq}) and one apical O atom (O_{ap})], one regular $Te1^{6+}O_6$ tellurate octahedron, one $Te2^{4+}O_3$ tellurite trigonal pyramid, one $Se^{4+}O_3$ selenite trigonal pyramid, two Pb sites (Pb1 and Pb2) and one H_2O site (O8). Two $Cu^{2+}O_5$ pyramids link to one another by sharing an O_{eq}–O_{ap} edge to form a Cu_2O_8 dimer. The $Se^{4+}O_3$ pyramid shares each of its basal O vertices with Cu_2O_8 dimers. The Se^{4+} at the apical vertex of the pyramid forms long bonds to O5 atoms within the $Te^{4+}O_3$ pyramid. The $Te^{4+}O_3$ pyramid shares two of its basal O vertices with Cu_2O_8 dimers and the third with a $Te^{6+}O_6$ octahedron. The $Te^{6+}O_6$ octahedron shares three vertices with Cu_2O_8 dimers and three vertices with $Te^{4+}O_3$ pyramids. The $Te1^{6+}O_6$ octahedron and the $Te2^{4+}O_3$ pyramids linked to it form a finite $Te^{6+}O_3(Te^{4+}O_3)_3$ cluster with a pinwheel-like configuration (Fig. 5).

https://doi.org/10.1180/mgm.2022.98 Published online by Cambridge University Press

Table 5. Atom coordinates and displacement parameters (Å^2) for tombstoneite.

	x/a	*y/b*	*z/c*	U_{eq}	U^{11}	U^{22}	U^{33}	U^{23}	U^{13}	U^{12}
Pb1*	0	0	½	0.0175(12)	0.0149(14)	0.0149(14)	0.023(2)	0	0	0.0075(7)
Pb2	0.73370(12)	0.73370(12)	0	0.0174(3)	0.0150(5)	0.0150(5)	0.0217(6)	0.0001(2)	−0.0001(2)	0.0072(5)
Cu*	0.3756(3)	0.3826(4)	0.8465(2)	0.0177(10)	0.0117(15)	0.0110(15)	0.0276(17)	0.0044(11)	−0.0029(11)	0.0036(12)
Te1	0	0	0.78402(17)	0.0120(5)	0.0094(7)	0.0094(7)	0.0173(11)	0	0	0.0047(3)
Te2	0.58885(17)	0.67484(18)	0.68160(9)	0.0136(3)	0.0118(7)	0.0110(7)	0.0188(6)	−0.0005(5)	−0.0004(5)	0.0061(5)
Se*	⅔	⅓	0.8918(2)	0.0152(11)	0.0116(13)	0.0116(13)	0.0224(19)	0	0	0.0058(6)
S	⅓	⅔	0.4009(7)	0.0197(19)	0.015(3)	0.015(3)	0.029(5)	0	0	0.0076(15)
O1	⅓	⅔	0.5205(19)	0.028(7)	0.033(11)	0.033(11)	0.018(13)	0	0	0.016(5)
O2	0.299(2)	0.501(2)	0.3593(13)	0.031(4)	0.051(11)	0.013(9)	0.036(9)	−0.010(7)	−0.007(8)	0.021(8)
O3	0.6779(18)	0.1701(18)	0.9602(11)	0.015(3)	0.011(7)	0.010(8)	0.020(7)	−0.005(6)	−0.008(6)	0.003(6)
O4	0.5316(19)	0.8351(18)	0.7255(13)	0.020(3)	0.016(8)	0.010(7)	0.032(8)	−0.013(6)	−0.007(7)	0.006(6)
O5	0.5918(18)	0.5867(19)	0.8184(12)	0.020(3)	0.013(8)	0.019(8)	0.024(7)	0.001(7)	−0.002(6)	0.006(7)
O6	0.8341(17)	0.8332(18)	0.6826(11)	0.015(3)	0.007(7)	0.008(7)	0.022(7)	0.000(6)	0.002(6)	−0.002(6)
O7	0.1656(18)	0.1737(17)	0.8760(11)	0.012(3)	0.016(8)	0.008(7)	0.016(7)	−0.007(5)	−0.009(5)	0.010(6)
O8	0.739(3)	0	½	0.042(8)	0.041(13)	0.07(2)	0.027(14)	−0.025(13)	−0.012(6)	0.034(11)

*Occupancies: Pb1 = $Pb_{0.497}Ca_{0.503(12)}$; Cu = $Cu_{0.984(13)}$; Se = $Se_{0.84}Te_{0.16(3)}$

Table 6. Selected bond distances (Å) in tombstoneite.

Pb1–O8 ×3	2.38(3)	Te1–O7 ×3	1.919(13)	Cu–O4	1.942(15)
Pb1–O6 ×6	2.709(13)	Te1–O6 ×3	1.965(14)	Cu–O7	1.948(15)
<Pb1–O>	2.599	<Te1–O>	1.942	Cu–O5	1.953(15)
				Cu–O3	1.995(14)
Pb2–O7 ×2	2.570(14)	Te2–O4	1.865(15)	Cu–O3	2.714(14)
Pb2–O5 ×2	2.592(15)	Te2–O5	1.869(15)	<Cu–O_{eq}>	1.960
Pb2–O3 ×2	2.662(15)	Te2–O6	1.968(14)		
Pb2–O7 ×2	2.673(13)	Te2–O4	2.393(15)	Se–O3 ×3	1.759(15)
<Pb2–O>	2.624	Te2–O1	3.033(16)	Se–O5 ×3	2.868(16)
		Te2–O2	3.093(18)		
S–O1	1.47(3)	Te2–O2	3.150(18)	Hydrogen bond	
S–O2 ×3	1.477(15)	<Te2–O_{short}>	1.901	O8···O2	2.67(2)
<S–O>	1.475	<Te2–O_{long}>	2.840		

Table 7. Bond-valence sums for tombstoneite. Values are expressed in valence units (vu).

	Pb1	Pb2	Cu	Te1	Te2	S	Se	H	Sum
O1					$0.07^{\times3\rightarrow}$	1.54			1.76
O2					0.06, 0.05	$1.52^{\times3\downarrow}$		0.24	1.88
O3		$0.24^{\times2\downarrow}$	0.42, 0.06				$1.20^{\times3\downarrow}$		1.92
O4			0.49		1.26, 0.35				2.10
O5		$0.28^{\times2\downarrow}$	0.47		1.25		$0.08^{\times3\downarrow}$		2.08
O6	$0.18^{\times6\downarrow}$			$0.92^{\times3\downarrow}$	0.98				2.08
O7		$0.30^{\times2\downarrow}$, $0.23^{\times2\downarrow}$	0.48	$1.00^{\times3\downarrow}$					2.01
O8	$0.38^{\times3\downarrow}$							$-0.24^{\times2\rightarrow}$	−0.10
Sum	2.23	2.11	1.92	5.78	4.03	6.09	3.84		

Multiplicity is indicated by ×→↓. Bond valences related to the Pb1 and Se sites are based on refined occupancies. Te^{6+}–O bond valence parameters are from Mills and Christy (2013). All others are from Gagné and Hawthorne (2015). Hydrogen-bond valences are based on O–O bond lengths from Ferraris and Ivaldi (1988). Negative values indicate donated bond valence.

The linkages noted above create a thick heteropolyhedral layer containing pockets, which host the Pb2 cations. The $Pb2^{2+}$ cation is eight coordinated to surrounding O atoms in the heteropolyhedral layer. The Pb2–O bonds cover a narrow range (2.570 to 2.673 Å); hence, the $Pb2^{2+}$ $6s^2$ lone-pair electrons are not stereoactive. Also of note, the Se^{4+} at the apical vertex of the $Se^{4+}O_3$ pyramid forms long bonds to O5 atoms within the same heteropolyhedral layer.

The SO_4 tetrahedron, the Pb1 site and the O8 H_2O site are located in the interlayer region of the structure. The O8 bonds only to Pb1. The three O2 atoms of the SO_4 tetrahedron each form two long bonds with $Te2^{4+}$ cations in the same heteropolyhedral layer and the O1 atom forms three long bonds to $Te2^{4+}$ cations in the adjacent layer. The Pb1 site is nine coordinated, forming three 2.709 Å bonds to O6 sites in one heteropolyhedral layer, three 2.709 Å bonds to O6 sites in the next layer and three 2.38 Å bonds to O8 H_2O sites in the interlayer. The Pb1 site is half occupied by Pb^{2+} and half occupied by Ca^{2+}. The joint occupancy appears to be necessary for bond-valence balance at the site. If only Pb^{2+} occupies the site, the BVS of the site is 2.66 vu, but with $Pb_{0.5}Ca_{0.5}$ occupancy, the BVS is 2.23 vu. Note that the distribution of bonds to the Pb1 site (see Fig. 6) suggests the possibility that the $Pb1^{2+}$ $6s^2$ lone-pair electrons may be stereoactive in two opposing directions, oriented 50% along **+c** and 50% along **−c**. Considering that Pb occupies only half of this site, the repulsive effect on the O6 atoms in each direction would only be 25% of that normally provided by lone pairs. It is also worth noting that the second highest electron

https://doi.org/10.1180/mgm.2022.98 Published online by Cambridge University Press

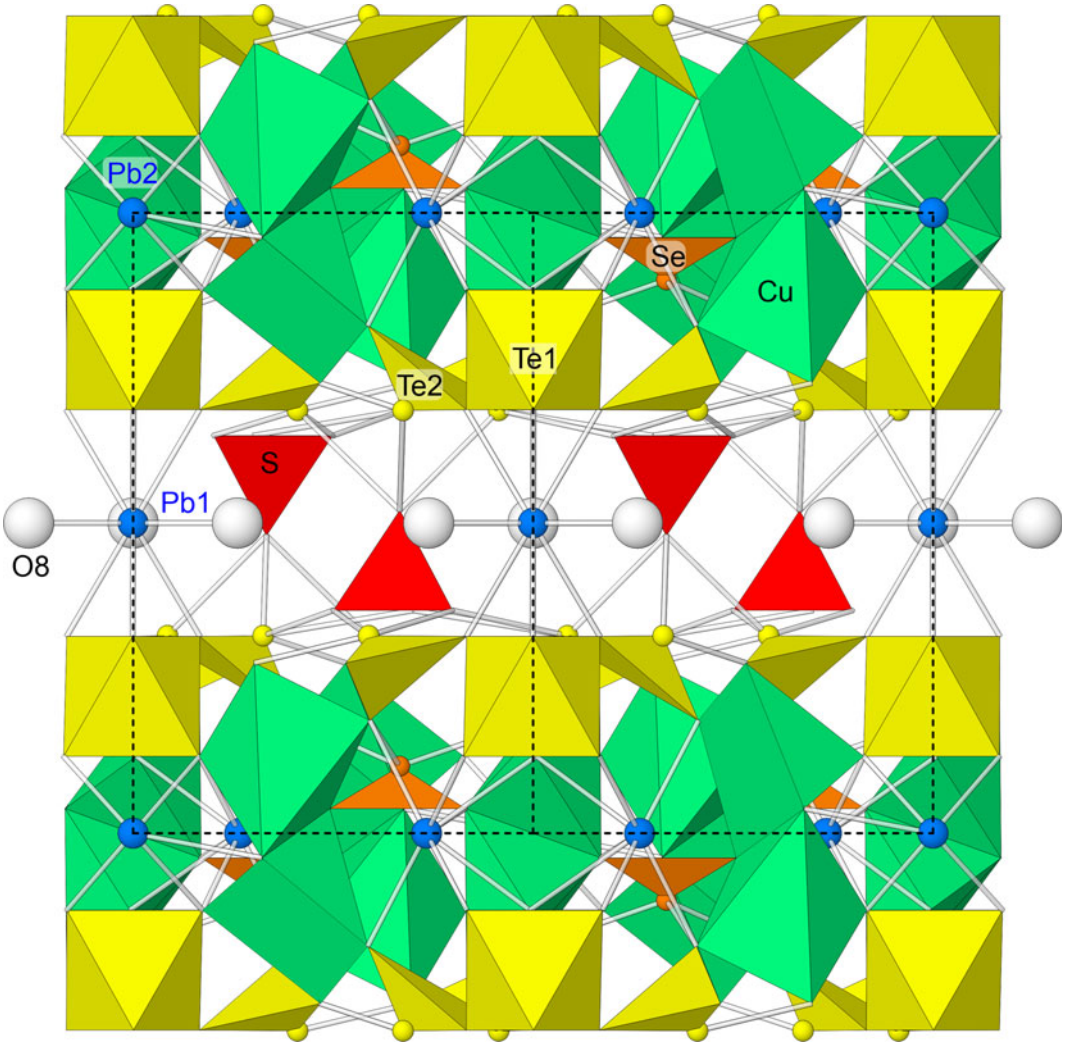

Fig. 4. The structure of tombstoneite viewed down [110] with [001] vertical. The unit cell outline is shown with dashed lines.

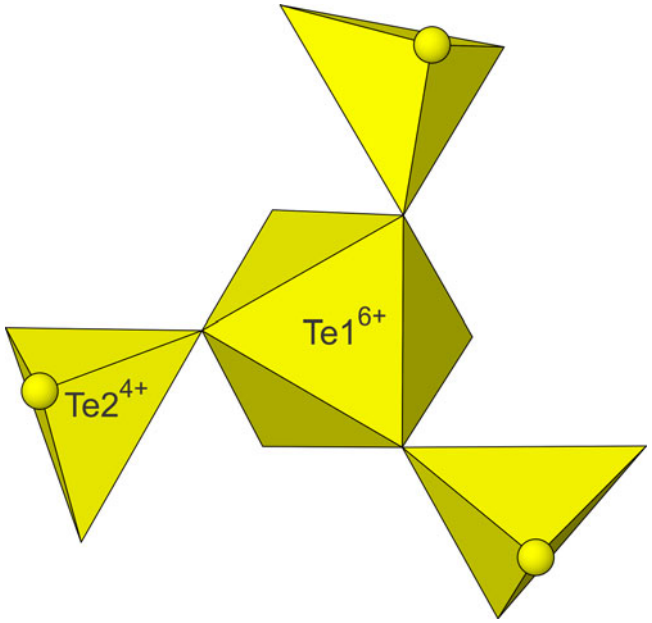

Fig. 5. The pinwheel-like $Te^{6+}O_3(Te^{4+}O_3)_3$ cluster in the structure of tombstoneite, viewed down **c**.

density residual (1.96 e/A^3) is located 0.79 Å from the Pb1 site along the **c** axis in both directions, approximately where one would expect electron density due to lone-pair electrons (see Fig. 6).

It is noteworthy that three different cations in tombstoneite have lone-pair electrons: Pb^{2+}, Te^{4+} and Se^{4+}. The lone-pair electrons of Te^{4+} and Se^{4+} are clearly stereoactive, resulting in their distinctive trigonal pyramidal coordinations; however, the $Pb2^{2+}$ lone-pair electrons are not stereoactive and it is not entirely clear whether the $Pb1^{2+}$ lone-pair electrons are. The complete coordinations of all of the cations (except S^{6+}) are shown in Fig. 6.

In the structural classification of Te oxycompounds of Christy *et al.* (2016), tombstoneite is a mixed-valence Te oxysalt, with both Te^{4+} and Te^{6+}. Christy *et al.* state that "*It is noteworthy that there are no structures in which* Te^{4+} *and* Te^{6+} *polyhedra are linked together into a finite Te–O complex.*" In fact, considering only the linkages between the $Te2^{4+}O_3$ pyramids and the $Te1^{6+}O_6$ octahedron in the structure of tombstoneite, it is the first known structure (natural or synthetic) with a finite complex that includes both Te^{4+} and Te^{6+} polyhedra. The only other mineral crystal structures that include both Te^{4+} and Te^{6+} polyhedra are: tlapallite, $(Ca,Pb)_3CaCu_6[Te_3^{4+}Te^{6+}O_{12}]_2(Te^{4+}O_3)_2(SO_4)_2 \cdot 3H_2O$, (mixed-valence phyllotellurate anion $[Te_3^{4+}Te^{6+}O_{12}]^{12-}$;

https://doi.org/10.1180/mgm.2022.98 Published online by Cambridge University Press

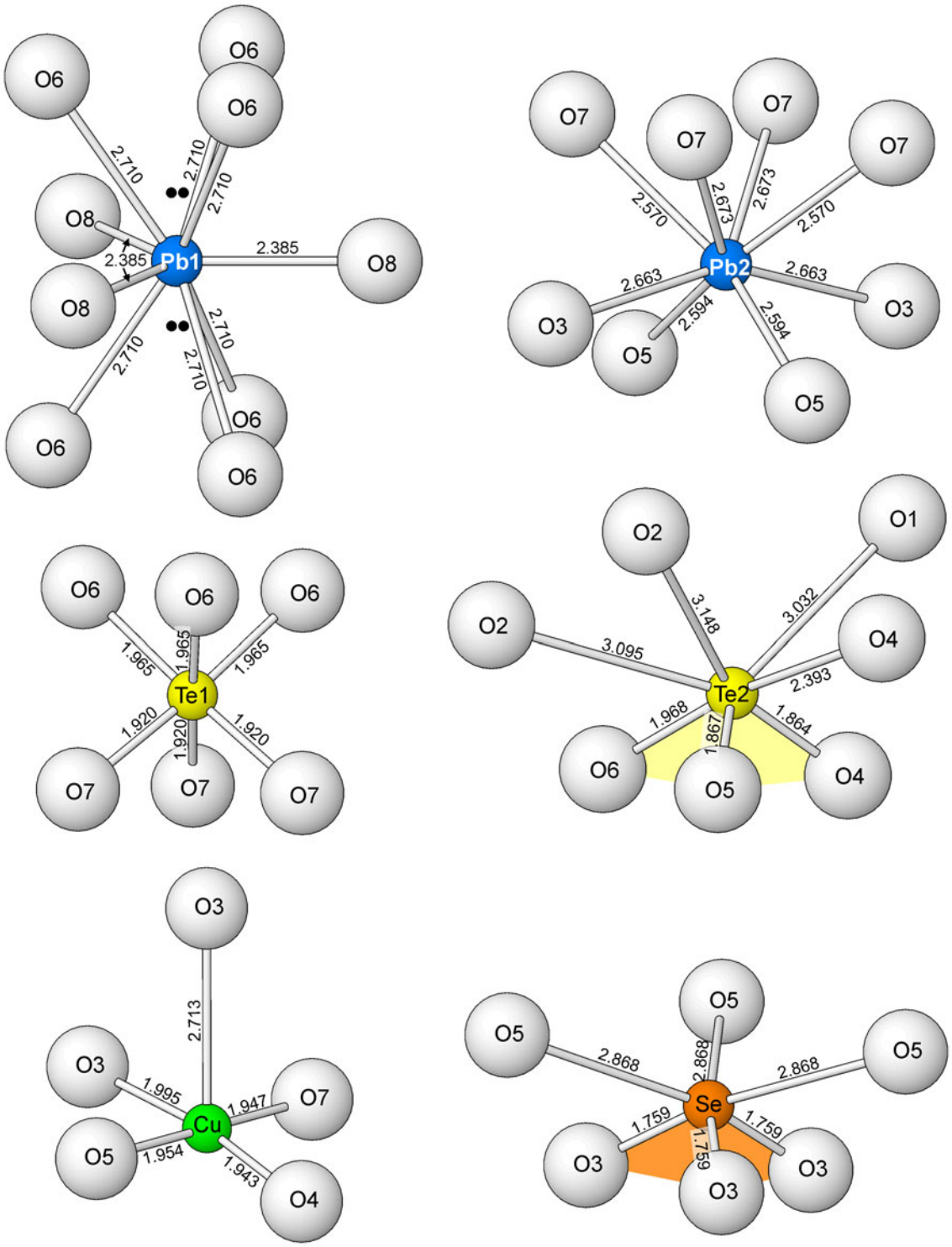

Fig. 6. The complete coordinations of all of the cations (except S^{6+}) in the structure of tombstoneite. The location of the electron density residuals possibly corresponding to the location of Pb1 lone-pair electrons are shown with double black dots. Note that, for the Te2 and Se coordinations, the three short Te2–O and three short Se–O bonds define the $Te^{4+}O_3$ (yellow) and $Se^{4+}O_3$ (orange) pyramids, respectively.

Missen *et al.*, 2019) and carlfriesite, $CaTe_2^{4+}Te^{6+}O_8$ (nanoporous $[Te_2^{4+}Te^{6+}O_8]^{2-}$ framework; Missen *et al.*, 2019), which both have their own new unique configurations.

Acknowledgements. Structures Editor and reviewers Oleg Siidra and Nicolas Meisser are thanked for their constructive comments on the manuscript. Preliminary Raman spectroscopy and EDS analyses at Caltech were funded by a grant from the Northern California Mineralogical Association. A portion of this study was funded by the John Jago Trelawney Endowment to the Mineral Sciences Department of the Natural History Museum of Los Angeles County.

Supplementary material. To view supplementary material for this article, please visit https://doi.org/10.1180/mgm.2022.98

Competing interests. The authors declare none.

References

Bindi L. and Cipriani C. (2004) The crystal structure of winstanleyite, $TiTe_3O_8$, from the Grand Central mine, Tombstone, Arizona. *The Canadian Mineralogist*, **41**, 1469–1473.

Christy A.G., Mills S.J. and Kampf A.R. (2016) A review of the structural architecture of tellurium oxycompounds. *Mineralogical Magazine*, **80**, 415–545.

Cooper M.A., Hawthorne F.C. and Back M.E. (2008) The crystal structure of khinite and polytypism in khinite and parakhinite. *Mineralogical Magazine*, **72**, 763–770.

Ferraris G. and Ivaldi G. (1988) Bond valence vs. bond length in O···O hydrogen bonds. *Acta Crystallographica*, **B44**, 341–344.

Gagné O.C. and Hawthorne F.C (2015) Comprehensive derivation of bond-valence parameters for ion pairs involving oxygen. *Acta Crystallographica,* **B71**, 562–578.

Higashi T. (2001) *ABSCOR*. Rigaku Corporation, Tokyo.

Hillebrand W.F. (1885) Emmonsite, a ferric tellurite. *Proceedings of the Colorado Scientific Society*, **2**, 20–23.

Kampf A.R., Mills S.J., Housley R.M., Rumsey M.S. and Spratt J. (2012) Lead–tellurium oxysalts from Otto Mountain near Baker, California: VII. Chromschieffelinite, $Pb_{10}Te_6O_{20}(OH)_{14}(CrO_4)(H_2O)_5$, the chromate analog of schieffelinite. *American Mineralogist*, **97**, 212–219.

Kampf A.R., Mills S.J. and Rumsey M.S. (2017) The discreditation of girdite. *Mineralogical Magazine*, **81**, 1125–1128.

Kampf A.R., Housley R.M., Rossman G.R., Yang H. and Downs R.T. (2020) Adanite, a new lead-tellurite-sulfate mineral from the North Star mine, Tintic, Utah, and Tombstone, Arizona, U.S.A. *The Canadian Mineralogist*, **58**, 403–410.

Kampf A.R., Mills S.J., Housley R.M., Ma C. and Thorne B. (2021) Tombstoneite, IMA 2021–053. CNMNC Newsletter 63. *Mineralogical Magazine*, **85**, https://doi.org/10.1180/mgm.2021.74

Kampf A.R., Mills S.J., Celestian A.J., Ma C., Yang H. and Thorne B. (2022) Flaggite, $Pb_4Cu_4^{2+}Te_2^{6+}(SO_4)_2O_{11}(OH)_2(H_2O)$, a new mineral with stair-step-like HCP layers from Tombstone, Arizona, USA. *Mineralogical Magazine*, **86**, 397–404.

Lam A.E., Groat L.A. and T.S. Ercit (1998) The crystal structure of dugganite, $Pb_3Zn_3Te^{6+}As_2O_{14}$. *The Canadian Mineralogist*, **36**, 823–830.

Mandarino J.A. (2007) The Gladstone–Dale compatibility of minerals and its use in selecting mineral species for further study. *The Canadian Mineralogist*, **45**, 1307–1324.

Mills S.J. and Christy A.G. (2013) Revised values of the bond valence parameters for Te^{IV}–O, Te^{VI}–O and Te^{IV}–Cl. *Acta Crystallographica*, **B69**, 145–149.

Mills S.J., Kampf A.R., Christy A.G., Housley R., Thorne B., Chen Y.S. and Steele I.M. (2014) Favreauite, a new selenite mineral from the El Dragón mine, Bolivia. *European Journal of Mineralogy*, **26**, 771–781.

Missen O.P., Kampf A.R., Mills S.J., Housley R.M., Spratt J., Welch M.D., Coolbaugh M.F., Marty J., Chorazewicz M. and Ferraris C. (2019). The crystal structures of the mixed-valence tellurium oxysalts tlapallite, $(Ca,Pb)_3CaCu_6[Te_3^{4+}Te^{6+}O_{12}]_2(Te^{4+}O_3)_2(SO_4)_2{\cdot}3H_2O$, and carlfriesite, $CaTe_2^{4+}Te^{6+}O_8$. *Mineralogical Magazine*, **83**, 539–549.

Missen O.P., Weil M., Mills S.J., Libowitzky E., Kolitsch U. and Stöger B. (2020) The crystal structures and Raman spectra of three new hydrothermally synthesized copper–zinc–oxotellurates (IV). *Zeitschrift für anorganische und allgemeine Chemie*, **646**, 476–488.

Missen O.P., Rumsey M.S., Mills S.J., Weil M., Najorka J., Spratt J. and Kolitsch U. (2021) Elucidating the natural–synthetic mismatch of $Pb^{2+}Te^{4+}O_3$: The redefinition of fairbankite to $Pb_{12}^{2+}(Te^{4+}O_3)_{11}(SO_4)$. *American Mineralogist*, **106**, 309–316.

Pertlik F. (1972) Der Strukturtyp von Emmonsit, $\{Fe_2[TeO_3]_3{\cdot}H_2O\}{\cdot}xH_2O$ (x=0–1). *Tschermaks Mineralogische und Petrographische Mitteilungen*, **18**, 157–168.

Post J.E., Von Dreele R.B. and Buseck P.R. (1982) Symmetry and cation displacements in hollandites: structure refinements of hollandite, cryptomelane and priderite. *Acta Crystallographica,* **B38**, 1056–1065.

Richmond W.E. and Fleischer M. (1942) Cryptomelane, a new name for the commonest of the 'psilomelane' minerals. *American Mineralogist*, **27**, 607–610.

Sheldrick G.M. (2015a) SHELXT – Integrated space-group and crystal-structure determination. *Acta Crystallographica,* **A71**, 3–8.

Sheldrick G.M. (2015b) Crystal structure refinement with SHELXL. *Acta Crystallographica,* **C71**, 3–8.

Tait K.T., DiCecco V., Ball N.A., Hawthorne F.C. and Kampf A.R. (2014) Backite, $Pb_2Al(TeO_6)Cl$, a new tellurate mineral from the Grand Central mine, Tombstone Hills, Cochise County, Arizona: description and crystal structure. *The Canadian Mineralogist*, **52**, 935–942.

Williams S.A. (1978) Khinite, parakhinite, and dugganite, three new tellurates from Tombstone, AZ. *American Mineralogist*, **63**, 1016–1019.

Williams S.A. (1979) Girdite, oboyerite, fairbankite, and winstanleyite, four new tellurium minerals from Tombstone, AZ. *Mineralogical Magazine*, **43**, 453–457.

Williams S.A. (1980a) Schieffelinite, a new lead tellurate–sulfate from Tombstone, Arizona. *Mineralogical Magazine*, **43**, 771–773.

Williams S.A. (1980b) The Tombstone district, Cochise County, Arizona. *Mineralogical Record*, **11**, 251–256.

Yang H., Gu X., Gibbs R.B. and Scott M.M. (2022) Murphyite, IMA 2021–107. CNMNC Newsletter 66; *Mineralogical Magazine*, **86**, https://doi.org/10.1180/mgm.2022.33